KC-135 AERO-OPTICAL TURBULENT BOUNDARY LAYER/SHEAR LAYER EXPERIMENT REVISITED

DR. J. CRAIG

SPECTRON DEVELOPMENT LABORATORIES, INC.

3303 HARBOR BLVD., SUITE G-3

COSTA MESA, CALIFORNIA 92626

MAJOR C. ALLEN

ARD

AIR FORCE WEAPONS LABORATORY

KIRTLAND AFB, NEW MEXICO 87106

ABSTRACT

This paper examines the aero-optical effects associated with propagating a laser beam through both an aircraft turbulent boundary layer and artificially generated shear layers. The data present comparisons from observed optical performance with those inferred from aerodynamic measurements of unsteady density and correlation lengths within the same random flow fields. Using optical instrumentation with tens of microsecond temporal resolution through a finite aperture, optical performance degradation was determined and contrasted with the infinite aperture time averaged aerodynamic measurement. In addition, the optical data were artificially clipped to compare to theoretical scaling calculations. Optical instrumentation consisted of a custom Q switched Nd:Yag double pulsed laser, and a holographic camera which recorded the random flow field in a double pass, double pulse mode. Aerodynamic parameters were measured using hot film anemometer probes and a five hole pressure probe. Each technique is described with its associated theoretical basis for comparison. The effects of finite aperture and spatial and temporal frequencies of the random flow are considered. The results presented represent five flights flown at altitudes from 1.8 km to 10.7 km and at Mach numbers from .32 to .79. Single pass phase deviations for the boundary layer were from .06 to .17 waves (at λ=.53μm) with piston and tilt components removed. Measured phase deviations for the artifically induced shear flows from .10 to .279 waves (at λ =.53μm) with piston and tilt components removed. However, when low order aberrations through coma were removed, the remaining

deviations were only .09 to .18 waves. This resulted in 33% to 250% increase in the Strehl ratio at 14 cm optical aperture. It was further shown that the low order aberrations corresponded to the longer wavelengths in the random flow and these waves propagated with a longer characteristic time than the higher order aberrations (200 to 1000 sec vs 50-100 sec or 1-5 khz vs 10-20 khz). Removing the low order spatial aberrations from the random flowfield up to a temporal frequency of 1 khz significantly improved optical propagation. In addition, the aerodynamic measurements could be correlated to the optical measurements to within 0.2 waves of tilt in the random flow, and aerodynamically measured correlation lengths matched the optical measurements when corrected for tilt and aperture scaling. Thus spatial optical performance parameters can be deduced from aerodynamic measurements.

Keywords

Shear layers, double pulsed holography, turbulent flow measurement, aero-optics, aerodynamic measurement, optical decomposition.

INTRODUCTION

Previous modelling and experimentation have characterized turbulent wavefronts propagated through aircraft boundary and shear layers. The techniques for the most part employed averaging assumptions that yielded results tending to maximize the distortion of optical wavefronts. All such distortions spread the radiation preventing beam focus to its diffraction limited spot size. The resulting aberrations were assumed to be isotropic and uncorrectable causing severe degradation to airborne astronomical observations, radiation sensing images, and laser beam propagation from aircraft. Better definition in both time and space of the aberrations to the flow was required to ascertain whether the averaged results here-to-fore determined and the resultant pessimistic view for practical applications were the appropriate conclusions. With proper knowledge of the actual flow, corrective techniques, either to the flow or to a propagating beam through the flow, could be applied to partially improve the beam or image to a level where operationally the system application could meet feasibility requirements.

This full scale experiment expanded on previous wind tunnel and airborne experiments described in the first four references. The three purposes of the experiment were (1) to more accurately quantify the boundary layer and artifical shear layer effects on optical propagation; (2) to compare and correlate aerodynamic measurement techniques with an optical diagnostic measurement technique across a turbulent fluid flow; and (3) to compare experimentally collected optical data

with theoretical scaling relationship for varying optical apertures.

The data are similar in nature to data collected in 1978 and reported in reference 1. Specifically the aerodynamic data were repeated using thin films on a five prong rake continuously movable along a radial centered on the laser beam propagation path to collect temperature fluctuations. The rake was replaced with a five hole pressure probe to collect pressure and mean flow velocity completing the aerodynamic measurements.

The optical measurements considered the temporal as well as spatial correlation by collecting 10 nanosecond pulse duration double pulsed holographic images at 5 double pulses per second and varying spacings between pulses (27 μsec to 2 ms). The beam size was analyzed at 1 to 15 cm. Coupling new measurement techniques with improved computerized data reduction and more precise numerical integrations result in aerodynamic and optical measurement self consistency that are uniformly higher than in reference 1.

The experimental setup for the five flight measurement program is shown in figure 1. Altitudes ranged from 1.8 to 10.7 km while Mach numbers varied from .32 to .79. A porous fence was located 7, 76 and 228 cm forward of the centerline of the measurement port, depending on the flight. The struts that hold the return mirror wing in place have curvature for zero lift. Although not observed previously, it was found at the highest mach numbers that weak vertical shocks set up between the struts so as to add some experimentally induced figure to the optical results. Therefore the 5.8 km .57 Mach conditions were con-

FIGURE 1

KC-135 AERO-OPTICS FLIGHT TESTS

AIRCRAFT BOUNDARY LAYER OPTICAL CHARACTERIZATION WITH DOUBLE PULSE HOLOGRAPHIC INTERFEROMETRY

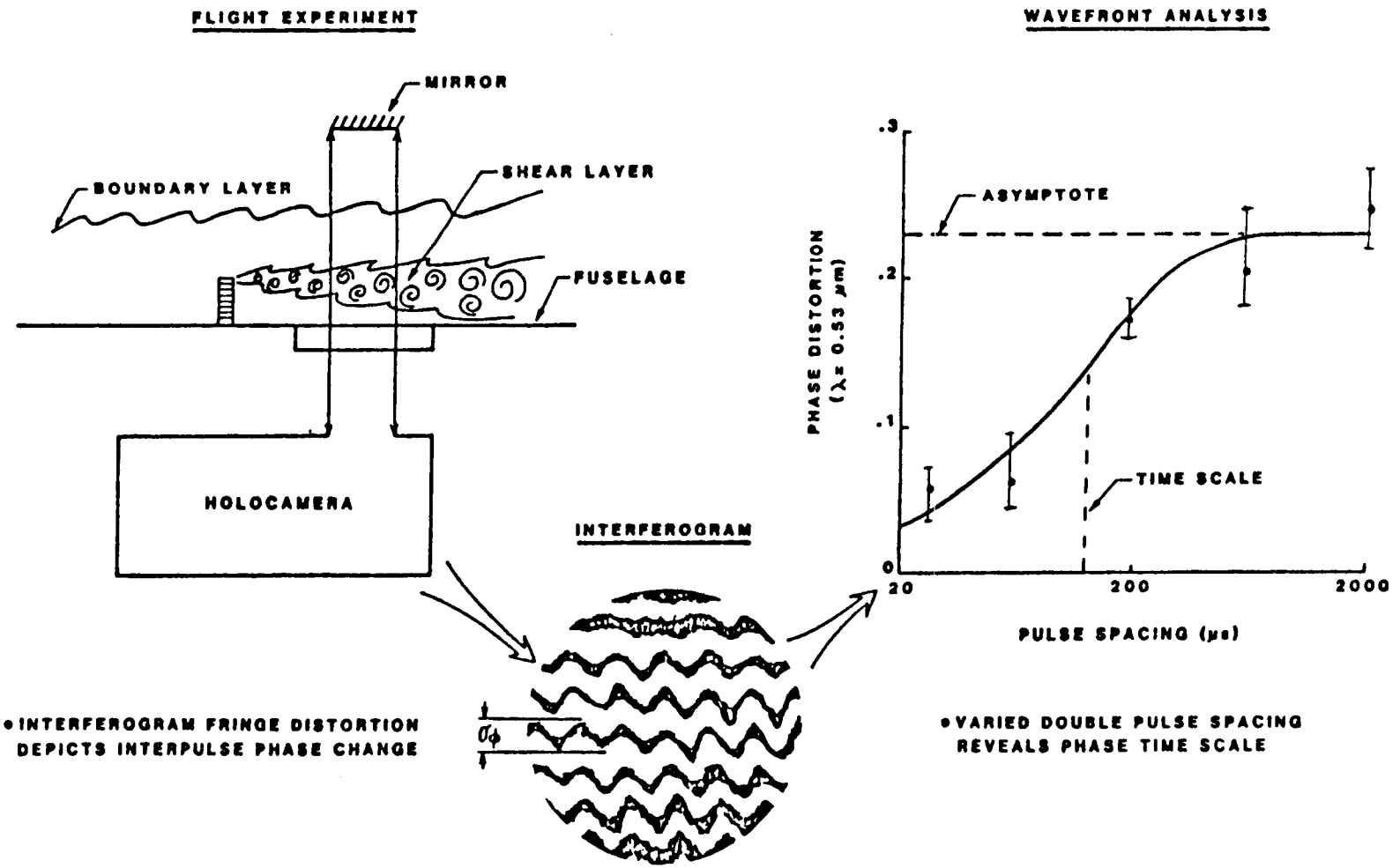

sidered as the baseline cases which excluded the shock perturbation. Although the qualititative average results remain unchanged, more precision and time sensitive data portend a significant decrease in aero-optical contribution to the system error budget with appropriate aeroflow corrective techniques. Further, data reduction improvements will allow significantly more data to be processed more accurately.

CONCLUSIONS

Four major conclusions from these test include the following: Aerodynamic phase variance averaged over time compares with the optical derived phase variance as corrected for infinite aperture to within the tilt compensation which is removed from the optical measurement. Comparing the optical measurement directly with clipped aerodynamic frequencies that relate to tilt, focus, astimatism and coma finds excellent agreement--.12λ versus .13λ . In addition the clipped aerodynamic data yield a correlation length that matches the optically derived length at 2 cm.

The aerodynamic measurements are time averaged along a central volume cylinder in front of the probe and thus time scales determined there cannot be substituted for optically measured timescales which relate the aeroflow as a nearly instantaneous phase screen.

Optical measurements at 15 cm aperture seem to infer that large spatial turbulent wavelengths propagate at slower flow velocities than shorter wavelength turbulence implying significant improvement in optical propagation could be attained with long wavelength relatively slow

compensation.

Finally the theory developed by Dr. Hogge in reference 5 is consistent with different clipped optical data.

Current measurement techniques are precise enough to quantify optical degradation due to aeroflows as a function of time. These data can be used to support (1) research in flow interogation and optical compensation, (2) design to alter the flow characteristics to remove or reduce the non-isotropic portion of the turbulence or (3) design of aeroflow modifiers to transfer isotropic turbulence to large scale turbulence and then couple that turbulence with low order optical corrective techniques. The results are possibly a key to successful use of optical systems on airborne platforms.

APPROACH

The aero-optics program involved several aspects; including instrumentation design and manufacture, development of data analysis procedures, flight test definition and conduct, and data reduction and interpretation. The instrumentation and data analysis procedures are discussed first, and the flight test is described in the remaining portion.

A double-pass holocamera was designed for installation at Station 1050 on an AF NKC-135. A customized frequency-doubled, Nd:YAG laser was used to record the double pulse holograms on 35mm film. The laser was designed and demonstrated to meet USAF airworthiness requirements. A mirror dithering system operating in a phase locked servo control

mode was used in the holocamera reference beam. This subsystem provided about 20 fringes of tilt on the interferogram either along the flow or normal to flow direction. An essentially automatic laser/holocamera control system was designed to provide high confidence and quality data acquisition. A typical double-pulse, hologram record consisted of about 100 double exposures with finite fringe. The double pulse measurement removes most system induced errors due to return mirror vibration and other vibration sources. A residual of one to three waves tilt above the induced tilt remain therefore the measurements must exclude tilt in the data processing. The double-pulse holographic interferograms were photographed in a ground laboratory, and the finite fringe interferograms were digitized on a new system developed by the Fringe Reduction Facility, FRF, at AFWL. The fringe detection system provided the ability to obtain quantitative phase statistics for turbulent flows. A time-differential interferogram analysis was developed to relate the double pulse interferogram data to the anemometer derived phase data.

The flight tests were designed to provide a comparison of the anemometer and optical diagnostic systems. This comparison was based on averaged statistically significant data which turned out to be for the optical data 15 samples per pulse spacing. An essential aspect of the experiment design was the generation of a flow object or flow field which could be appropriately sampled through the holocamera optical aperture. To obtain adequate spatial sampling, a flow field structure with small length scales was required. The MID FENCE (76 cm) position

was identified as most appropriate. The flow length scales in the ambient boundary layer are quite large at the aircraft measurement station; however, the porous fence disrupts the ambient boundary layer flow along the fuselage. Immediately downstream of the fence (NEAR FENCE at 8 cm), the flow field is composed of a shear layer at the other edge of the fence separating the low speed flow through the fence and the high speed boundary layer flow over the fence. The composite aspects of this flow region make it less desirable for optical comparison. However, further downstream the shear layer has entrained or consumed most of the extraneous turbulence, and this position (MID FENCE) is selected as the primary flow object for data comparison. The optical data here samples up to 75% of the spatial frequencies. In addition, since the flow has not quite reattached at this point, the shear layer turbulence structure is nearly isotropic, particularly in comparison to bounded turbulent flows. At the final fence position (FAR FENCE) (228 cm), the reattaching shear layer has grown considerably in thickness and optical distorting power. A complete double-pulse hologram data set was acquired for three fence positions and through the ambient boundary layer at four flight conditions. The interferograms recorded for increasingly longer pulse spacing revealed stronger fringe distortions as was expected. The ambient boundary layer (NO FENCE) was observed to be the weakest phase distorting object, and with the fence installed, the distortion was observed to increase with distance from the fence. The growth rate of the distortion with distance is increased at higher Mach number.

Double-Pulsed Nd:YAG Laser

A Molectron Corporation Model MY-30 frequency doubled Nd:YAG laser as supplied was intended for laboratory use and consisted of a Nd:YAG oscillator and amplifier and KDP frequency doubler. The unit was designed for operation on 208 volt, 60 cycle AC three phase prime power, and utilized a tap water cooled heat exchanger.

A careful characterization of the laser prior to modification demonstrated that the unit was capable of about 200 mJ/pulse operation at 0.532 μm at 10 Hz, with a coherence length of approximately 1 cm (linewidth of $0.1cm^{-1}$). No double pulse capability existed in the factory unit.

Extensive modifications of the laboratory unit included pulse forming networks, double pulsing electronics, flashlamp simmer circuits, and pockels cell trigger circuits. Airborne power supplies were specified and purchased for operation at 120 VAC 400 cycle three phase aircraft power and 28 VDC.

An environmental housing for the laser optical system was designed and fabricated. Extensive mechanical modifications were incorporated to meet a U. S. Air Force 9g forward load crash requirement. Modifications of the laser output optical path were incorporated to meet aircraft configuration requirements. Vibration testing included an operational demonstration after two cycle of a 2g, 5-500 Hz shake. The laser optical unit was cycled over a ΔT of 40^{o} F and post-test operation was demonstrated.

A freon to water airborne cooler and control system was designed

and incorporated into the NKC-135 aircraft environmental control system.

Double-Pass Holocamera

A custom holographic camera was designed and fabricated for the aero-optics experiment. The optical system consists of an object beam and reference beam. The object beam is expanded to 16 cm diameter and is projected (through an optical port) out of the aircraft through the shear layer to a return mirror mounted on an airfoil wing, thus double passing the flow. The reference beam is pathmatched to the object beam to within .5 cm. A two-axis dither mirror control system is contained in the reference beam to place reference tilt fringes on the resulting holographic interferograms.

The entire optical system is housed in a structure to make the camera light-tight, keep the optical system clean, and meet USAF airworthiness requirements. Access to the holocamera for adjustment in flight is facilitated by twelve hatches which are integral to the top cover.

Features of the camera include:

35mm roll film operation

automatic film writing (frame number) via LED film printer

automatic monitoring of object and reference beam energy and ratio

automatic X and Y dither mirror control via phase locked servo controlled loop

temperature monitoring at three points

vibration monitoring (via accelerometers) at two points

interchangeable 4 x 5 glass plates with 35mm roll film to obtain single-pulsed holograms

transceiver optical design for object beam utilizing common path optics

apertures and light baffles to minimize stray radiation and outside aircraft ambient light

monitoring of aircraft fuselage expansion for various flight conditions

reference beam remote pathmatch adjustment to compensate fuselage growth

mechanical design capable of withstanding 9g forward crash load

airworthy wiring and electronic components

Holographic Reconstruction

After developing, the flight hologram film reels were inserted in a custom film transport within the reconstruction system. The reconstruction beam was obtained from a spatially filter HeNe laser. The holocamera reference beam divergence was reproduced in the

reconstruction system. The reconstructed object beams which constitute the interferogram are spatially filtered to increase fringe contrast. The interferogram aperture is focused on the camera film plane. The aperture is the large lens in the object beam telescope. The interferograms were photographed on Tech Pan film and developed with HCL110F. The film and the developing process were selected to achieve moderate fringe contrast and sufficient exposure dynamic range. Sufficient dynamic range is required to record interferogram intensity variation across the aperture.

Aerodynamic Procedure

Turning now to the aerodynamic procedure. A movable five fingered thin film temperature rake or five-hole pressure probe was inserted into the artificial shear layer along the centerline of the optical measurement. Obtained from this data through the differential form of the equation of state was the density variation of the flow and mean velocity and pressure data. The thin film temperature data was recorded in the FM mode with the films configured to record from 0 to 100 Khz. The pressure probe recorded ambient and total steady state pressure over about 10 second spans. This data, when properly correlated with velocity data, yielded the time averaged density variation and correlation lengths along the centerline and thus a time averaged phase variance. Assuming homogeneity across the flow an infinite aperture Strehl ratio was derived which is a measure of the intensity dispersion caused by the flow. This is the worst case Strehl assuming no temporal or spatial correction and isotropic turbulence.

Fringe Detection and Wavefront Analysis

The interferogram fringe detection and wavefront analysis was performed by the Fringe Reduction Facility at AFWL. The primary data reduction was performed on a set of eighteen interferograms (nine with flow direction fringes and nine with normal to flow direction fringes) for each of 80 test conditions (flight condition [4], model installation [4], and pulse space [5]).

The fringe detection camera was configured with a film transport which could be rotated about the optical axis. The image was detected by scanning a linear photodiode across the image. The film transport was oriented such that the nominal fringe direction was normal to the photodiode array or parallel to the scanned direction. Fringes were numbered from zero to N across the aperture. The maximum fringe number was typically 20, except for the short pulse spacing, 27 μs, for which six or eight fringes were introduced.

The fringe detection system was designed to trace the fringe edges of a few fringes in each scan across the aperture. In the instances where fringe edges were lost in noise, the system would mark the point and continue until the noise dropped and the fringe edge detection was regained. After all identified fringe coordinates had been detected by automatic means, the operator would assist the patching of drop-out regions.

The fringe detection scheme locates fringe center coordinates across the interferogram. After averaging across several (~10 scan), average fringe centers were connected by the computer into the fringes

along the scan. When the computer could not connect the fringe center, it appealed to human intervention. The phase is constant along fringes and increases by one wave from one fringe to the next fringe. The phase map, as originally detected, is a high frequency random distortion imposed on a highly tilted wavefront (i.e., $\simeq$ 20 waves).

Since the wavefront phase is known only along fringe centers, the nonuniform phase map is interpolated onto a uniformly spaced grid. The grid interval was 128 x 128 or about 0.1 cm spacing in each direction over 15. cm aperture which is ample accuracy to resolve low order Zernike times. Zernike polynomials are orthogonal polynomials that define optical aberration over a phase front (e.g., tilt, focus, coma).

The first step in the wavefront analysis is to determine the Zernike polynomials components of the interferogram and the residual variance using a least square fit of the data for a selected order of fit. This analyses used piston and tilt removed and the residual variance denoted, σ^2_{0-2} and piston tilt focus astimatism and coma removal with residual variance denoted σ^2_{0-8}. So experimental error in tilt was removed first and the low order optical terms were determined to 10% accuracy.

Time Differential Interferogram Analysis

The fringe distortion recorded on the double-pulse holographic interferograms represents a time-differential phase, $\Delta\phi$, or

$$\Delta\phi(x,t) = \phi(x,t) - \phi(x,t-t') \qquad (1)$$

where t' is the laser pulse spacing. A correlation analysis is developed in Ref. 2 in which Equation 1 is expanded to provide a relation between the differential, $\Delta\phi$, and absolute, ϕ, phase correlation functions. Specifically, the two point, $\tilde{x}_1$ and $\tilde{x}_2$, spatial correlation function derived from the interferograms is shown to be

$$R_{\Delta\phi}(\tilde{x}_1, x_2) = 2\,(R_\phi(\tilde{x}_1, \tilde{x}_2) - R_\phi(\tilde{x}_1, \tilde{x}_2, t')) \tag{2}$$

where $\tilde{x}_1$ and $\tilde{x}_2$ are the cross aperture coordinates at which the phase correlation is being computed. The RHS of Equation 2 is twice the difference of the spatial and space-time phase correlation functions, where the time delay in the space-time correlation is equal to the double-pulse spacing. The major result is obtained from Equation 2 by equating $\tilde{x}_1$ and $\tilde{x}_2$ and letting the pulse spacing become sufficiently long that the space-time correlation function is zero. The differential phase variance, $\sigma^2\Delta\phi$, is twice the conventional variance, or

$$\sigma^2\Delta\phi = 2\sigma^2\phi \tag{3}$$

These temporal phase variances are equivalent to spatial variances for homogeneous phase statistics. Hence, the desired result is that the temporal variance equivalent to that derived from anemometer data is obtained by ensemble averaging the spatially derived differential phase variance, or

$$\sigma^2\phi = \frac{1}{2}\left\langle \sigma^2\Delta\phi \right\rangle \Big|_{t' \to \infty} \tag{4}$$

The temporal phase statistics are obtained from the double pulse holograms recorded at shorter pulse spacing. Equation 2 is evaluated at zero spatial offset, $\tilde{x}_1 = \tilde{x}_2$, and the temporal phase correlation function, R (t), is obtained from the shorter pulse spacing interferograms, or

$$R\phi(t) = \frac{1}{2}\left(\left\langle \sigma^2 \Delta\phi \right\rangle \Big|_{t' = +\infty} - \left\langle \sigma^2 \Delta\phi \right\rangle \Big|_{t' = t} \right) \tag{5}$$

The RHS of Equation 5 is the difference between the ensemble average of the long pulse spacing variance (i.e., Eqn. 4) and a shorter pulse spacing, t' = t, variance. The form of the correlation function has been assumed exponential in the data reduction, i.e.,

$$R\phi(t) = \sigma^2\phi_o e^{-t/t_o} \tag{6}$$

where the variance, $\sigma^2\phi_o$, and the time scale, t_o, are the fit parameters obtained by least squares analysis or

$$\sigma^2 = \sigma^2\phi_o (1 - e^{-t/t_o}) \tag{7}$$

After examining the statistics of a single data set in great detail, the number of interferograms required for ensemble averaging at each pulse spacing was selected to be 18 or 90 over the 5 time spacings. From optical theory, the phase variance can be decomposed into a series of orthogonal Zernike coefficients.

$$\sigma^2 = \sum_{i=o}^{N} a_i P_i \tag{8}$$

By application of the theory of superposition equation (7) applies to the Zernikes

$$P^2_i = P_{2_{i_{\phi_o}}} (1 - e^{-t/t_{oi}}) \qquad (9)$$

where each Zernike term has its own time constant. This implies that low order Zernike may respond differently in time than higher order terms.

Flight Test

Six flights were flown from Kirtland AFB and data was taken over White Sands Missile Range, New Mexico, on an Air Force NKC-135 aircraft in the spring of 1984. For each flight, the fence was mounted in a single position and data were acquired at four flight conditions. The fence positions were 8.0, 76., and 38, cm upstream of the measurement station, and for one flight, the fence was not installed. The flight conditions were selected to produce an altitude/Mach number variation at constant Reynolds number (unit Reynolds number = 6.0×10^6/M or running length Reynolds number = $175. \times 10^6$. The fence positions were selected to produce desired flow configuration at the measurement station.

One complete data record was obtained at each flight condition. A data record consisted of a 100 hologram set at each pulse spacing with 45 frames taken in vertical and horizontal fringe orientations, and the remaining ten with infinite fringe spacing. Pulse spacing from 27 μs to 2.0 ms, were obtained.

Data were recorded in eight-minute, steady level flight legs within the controlled airspace.

Data Reduction

The primary optical data reduction approach has been the determination of phase correlation functions. The temporal dependence is obtained by least squares analysis of the time-differential interferograms, and the spatial dependence is obtained by ensemble averaging the products of spatially shifted wavefronts. These analyses result in a phase variance, time scale and length scale.

For large aperture sampling, the resulting phase variance is equivalent to that derived from the anemometer diagnostics. Further, to ascertain the dependence on sampling aperture, the temporal correlation functions are obtained for partial aperture regions. Finally, to obtain the temporal behavior of various low spatial order terms (i.e., focus, astigmatism, and coma), the temporal variance of several low order Zernike coefficients has been obtained for a set of time-differential interferograms. The least squares analysis applied to these Zernike data sets results in, for example, a focus amplitude and time scale.

Time Dependent Phase Correlations

The spatial phase variance samples obtained from time-differential interferograms are obtained by the fringe detection and wavefront analysis techniques described earlier. Actually, the residual variance is

provided after removing piston and tilt components (i.e., σ^2_{0-2}) and after removing Zernike coefficients through a coma aberration (i.e., σ^2_{0-8}). Ninety samples are used in the least squares analysis to obtain the phase variance and time scale (i.e., Equation 6) of the exponential correlation function. The least squares analysis provides the best fit to the following equation:

$$\frac{\sigma^2 \Delta\phi(t')}{8} = \sigma^2_{\phi(t')} = \sigma^2_{\phi_0} (1 - e^{-t'/t_0})$$

where the factor of 8 represents the double pass factor of 4 and the double pulse factor of 2.

The least squares data fit to σ_{0-2} and σ_{0-8} data sets for the 5.8 Km/0.57M MID FENCE position are shown in Figures 2a and 2b. Eighteen data points are plotted at each pulse spacing, and the resultant fit is plotted. For the σ^2_{0-2}, the asymptote is 0.21 waves and the time scale is 192 μs; whereas after removing low order spatial terms (through eighth order Zernike), the asymptote variance is reduced to 0.14 waves with a time scale of 90 μs. The 30 percent reduction in phase variance produces a sizable improvement in Strehl ratio (i.e., from 0.17 to 0.48, respectively, if the exponential relation is assumed valid). For this case, the Strehl ratio improves a factor of three with the removal of correction of low order distortion. The averaged time scale for σ_{0-2} (192 μs) is noted to be significantly larger than the σ_{0-8} value (90 μs). This is because the lower Zernikes propagated slower than the higher order values. Removing the lower Zernike leave

FIGURE 2a Tilt Removed Least Squares Analysis

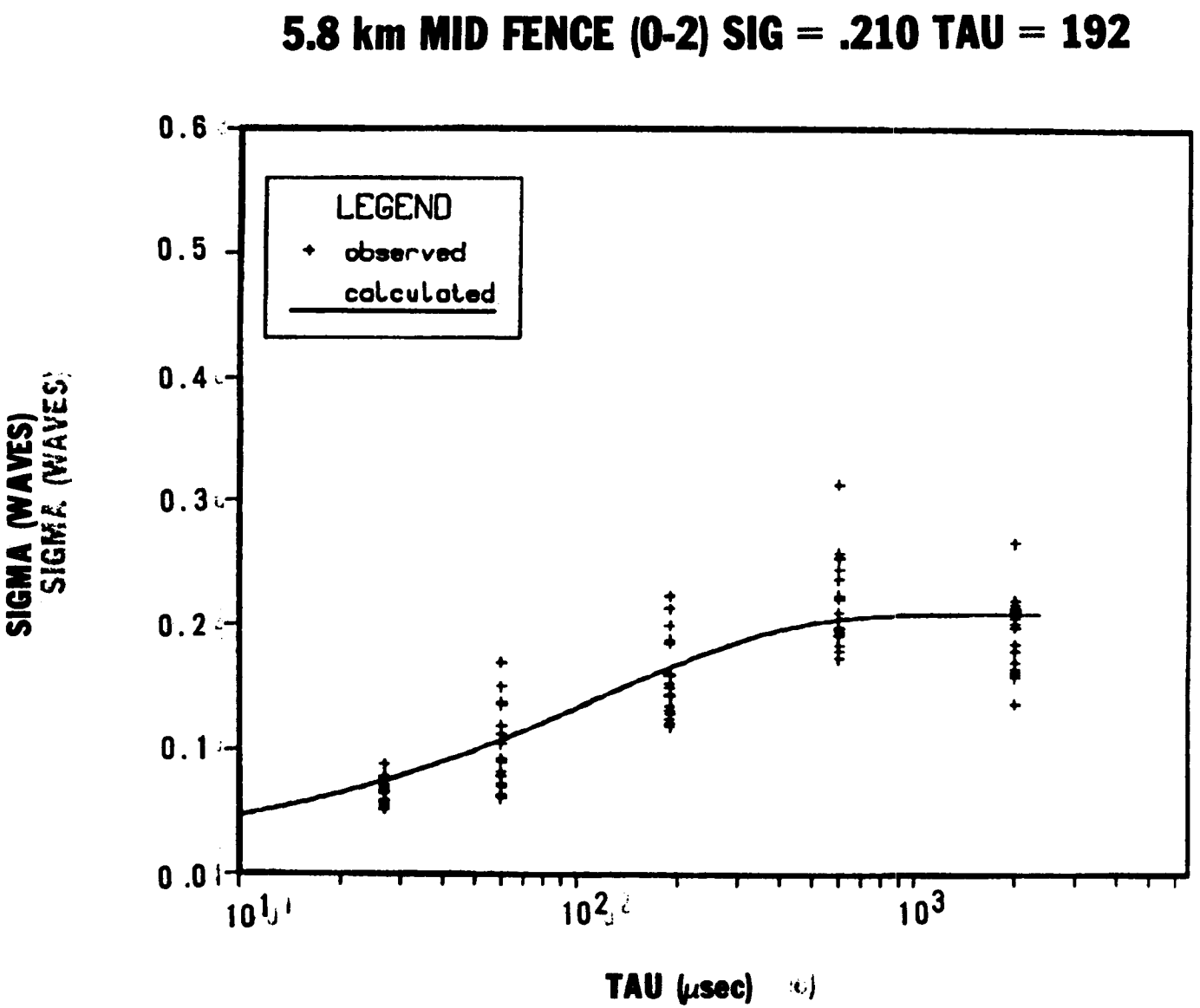

an average time scale that is lower than before. Applying Equation 8 can determine the actual correction frequency for each Zernike term necessary to obtain the average values obtained from the fit.

The entire flight test matrix and the ground calibration data are shown in Table 1. The ground calibration data reveal a noise level of about $\lambda/20$ to $\lambda/30$ for σ_{0-2} and σ_{0-8} data sets. The calibration data reveal no pulse spacing dependence. Strehl improvement of between 30% and 250% at 14 cm aperture was seen, the average time scale is consistently less for the coma removed data indicating short wavelength aberrations appear to move faster than longer wavelengths. The signal-to-noise ratio is poorest at low altitude/Mach number with the boundary layer flow object, and is best for all of the higher altitude/Mach number conditions for the FAR FENCE flow object. As a result of low signal-to-noise for the 1.8 and 5.8 Km boundary layer data, the time scales are judged not applicable.

Space Dependent Phase Correlations

The dependence of the phase correlation on the spatial offset is obtained for a single flight condition, as the computation requires handling of eighteen phase maps each containing 10^4 grid points. The phase spatial resolution is 128 x 128 grid points, or 0.1 cm in the 15 cm aperture. The phase correlation in space is derived from ensemble averages of the product of spatially shifted wavefronts, or

$$R_{\phi}(x',y') = \frac{\phi(x,y)\ \phi(x-x',y'y')}{\langle\phi(x,y)^2\rangle}$$

TABLE 1

HOLOGRAPHIC RESULTS

σ, τ, STREHL (WAVES, μSEC, RATIO)

(PISTON - TILT REMOVED
PISTON THROUGH COMA REMOVED)

ALTITUDE/MACH (km)	BOUNDARY LAYER	NEAR (8 cm)	MID (76 cm)	FAR FENCE (228 cm)
1.8/.32	.057, 2, .880 .042, 37, .933	.104, 166, .652 .093, 43, .711	.114, 90, .599 .084, 42, .757	.125, 266, .540 .087, 115, .742
5.8/.57	.113, 17, .604 .084, 8, .757	.181, 86, .274 .157, 83, .378	.210, 192, .175 .137, 90, .477	.279, 265, .046 .180, 122, .278
8.8/.68	.170, 166, .320 .122, 87, .556	.172, 91, .311 .149, 78, .416	.189, 129, .244 .142, 92, .451	.260, 152, .069 .184, 102, .263
10.7/.79	.137, 141, .477 .104, 80, .652	.173, 78, .307 .150, 61, .411	.185, 144, .259 .127, 45, .529	.265, 211, .063 .175, 113, .298
GND CAL	.041, 2, .936 .073, 1600, .810			

The ensemble averaging has been performed for the 2.0 ms pulse spacing data broken into vertical and horizontal fringe orientation sets.

The two-dimensional correlation functions obtained from each data set is plotted in slices through the x and y axis in Fig. 3. In general, the correlations decay to zero at about 4 cm shift and reach a lower limit of -0.1 at 6 cm. The spatial length scales are equal in both directions (i.e., about 2 cm), as judged by the shift coordinate at the point where the correlation is e^{-1}. This would indicate that the phase distortion is fairly isotropic.

Partial Aperture Phase Variance

The phase distortion observed through reduced aperture diameters have been determined by cropping the interferogram in the data reduction step. The full aperture data as discussed were actually cropped to 90 percent of the holocamera aperture of 14 cm diameter. The partial aperture diameters were 8.0 cm, 5.0 cm, and 2.5 cm. The wavefront analysis is designed to remove both tilt components before computing the residual phase variance, σ^2_{0-2} or phase deviation σ_{0-2}. New tilt components are computed for successively smaller apertures. The residual phase variance is also computed after removing the first eight Zernike coefficients, and this variance is denoted, σ^2_{0-8}.

The partial aperture phase variances have been obtained for all four model configurations at 5.8 Km/0.57M. The σ_{0-2} data (Table 2) for each model configuration reveal increasing distortion with increasing aperture diameter. This indicates that a larger portion of

TABLE 2

5.8 km OPTICAL CLIP ANALYSIS

σ WAVES (.53), τ μSEC, STREHL RATIO

(PISTON-TILT REMOVED
PISTON-COMA REMOVED)

APERTURE DIAMETER (cm)	BOUNDARY LAYER	NEAR	MID	FAR FENCE
2.5			(.051, 66, .902 .025, , .976)	
5	(.055, 28, .887 .032, 2, .960)	(.118, 111, .577 .066, 85, .842)	(.097, 109, .690 .055, 63, .887)	(.120, 121, .566 .070, 81, .824)
9	(.084, 29, .757 .059, 37, .872)	(.155, 91, .387 .117, 78, .939)	(.154, 142, .392 .099, 93, .679)	(.205, 182, .190 .120, 92, .566)
14	(.113, 17, .604 .084, 8, .757)	(.181, 86, .274 .157, 83, .378)	(.210, 192, .175 .137, 90, .477)	(.279, 265, .046 .180, 122, .278)
INFINITE (AERO)		.252/ / .082	.263/ / .065	.904/ / 0

FIGURE 3 Spatial Correlation Function Through X and Y Axes. 5.8 km/0.57M Flight Condition, Mid Fence

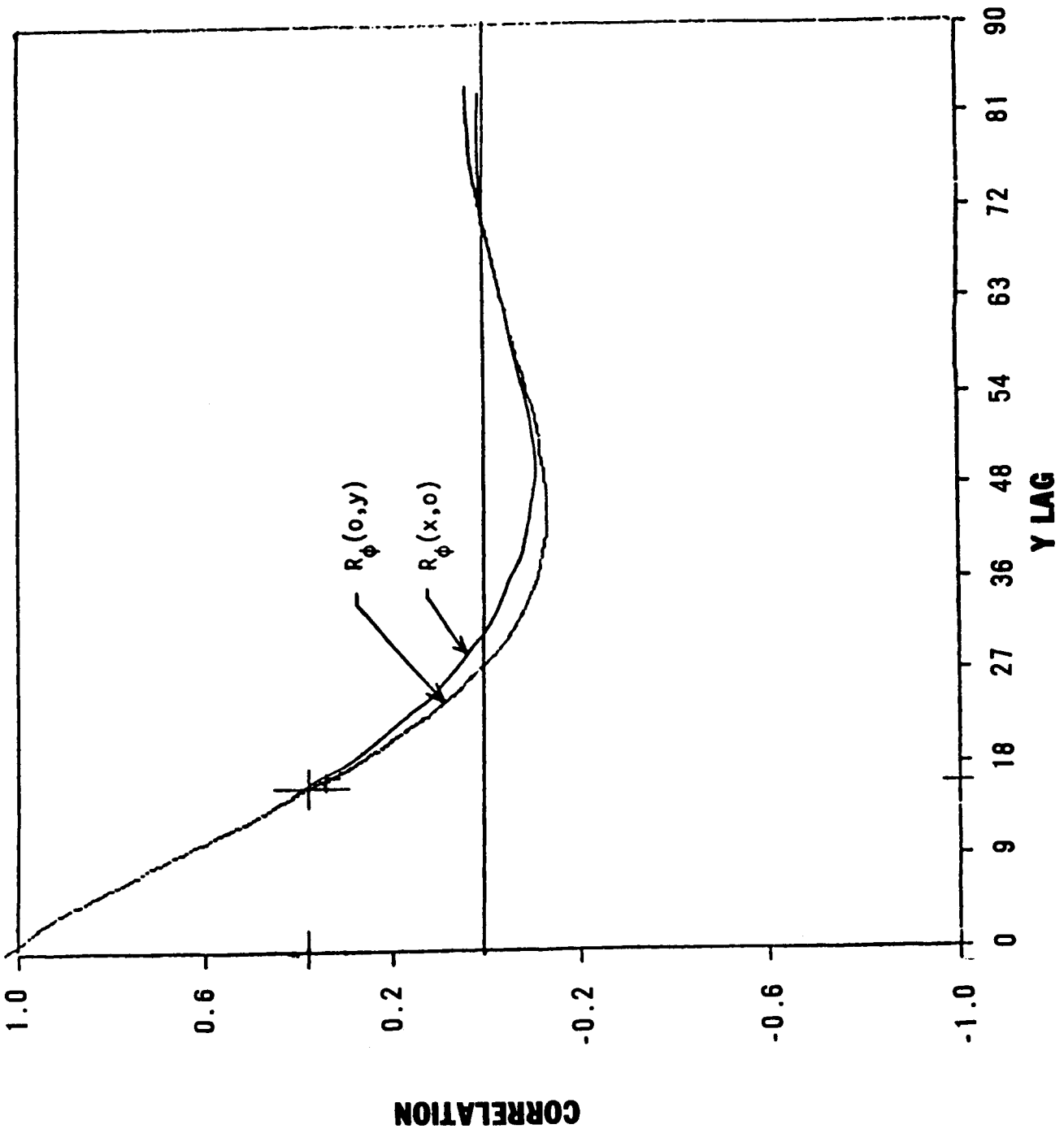

the spatial frequency phase spectrum is sampled or detected as the aperture diameter is increased. The boundary layer flow object exhibits the best optical quality. The NEAR and MID FENCE flow objects exhibit similar trends; however, the NEAR FENCE data decreases at a slower rate with aperture size, indicating that much of its spectral strength must be at high spatial frequency. This observation is in agreement with the anemometer scale size data.

The ratio of the low order removed deviation to the tilt removed deviation, $\sigma_{0-8}/\sigma_{0-2}$, increases from about 57 percent at 5.0 cm aperture to about 72 percent at 13.5 cm aperture. This trend suggests that for larger apertures the phase distortion moves to higher spatial frequencies relative to the apertures size and, in particular, the low order Zernike terms become less significant for correction. The time scale is observed to increase with aperture size, also suggesting the large scale structures within the flow have lower temporal frequencies.

The temporal sampling variation was sufficient to detect all of the tilt removed spectrum as the phase variance was clearly observed to asymptote at large pulse spacing. In contrast to the temporal sample, the spatial sampling variation was not sufficient to detect the entire spatial frequency spectrum, as a result, the phase variance did not asymptote within the sampled aperture range (i.e., up to 15 cm diameter). Later, the propagation analysis of Hogge will be employed with the anemometer data to estimate the infinite aperture size for all four flow objects at the 5.8 Km/0.57M flight condition.

C-6

Zernike Spatial Decomposition

Turning attention to the low order Zernikes which is corrected can result in a 15 to 40% beam quality improvement. Table 3 shows the peak deviation of each Zernike term. Since the flow is random the mean of each term is very close to zero. Therefore the deviation of each term was used as the measure of merit. For a typical case, a 2σ peak to peak variation is on the order of 1 wave or 4 times the values listed. Correction frequencies are the inverse of the vibration time listed or 2-5 KHz at 14 cm aperture. Large optics would have somewhat lower correction frequencies but may not get the same large percentage improvement because the characteristic size of the turbulence may be near maximum at 15-20 cm. This implies that for large apertures the significant spatial bandwidth may extend to fairly high orders. The data was collected by fitting (as per equation 9) the $1\text{-}\sigma$ value of the pertinent Zernike term obtained from statistical analysis of the interferograms for each time spacing and flight condition.

Aerodynamic/Optical Comparisons

A major flight test objective was to provide optical data for validation of hot-wire anemometry based characterizations of turbulent flow optics. The anemometer approach is to derive the optical phase variance by path integration of the refractive index statistics, as determined from the hot-wire anemometer. For spatially homogeneous flows, the temporal phase variance is also indicative of a spatial phase variance as would be subjected to a large aperture wavefront.

TABLE 3

TABULATED LOW ORDER ZERNIKE ANALYSIS

P (WAVES), t(μs) for 14 and 8.9 cm Aperture

ALTITUDE/ MACH (km)		BOUNDARY LAYER	NEAR	MID	FAR FENCE
1.8/.32		P3, t3 P4, t4 P5, t5 P6, t6		.067, 140 .147, 458 .093, 190 .092, 230	
5.8/.57		.074, 44 .064, 23 .241, 4800 .081, 70	.102, 147 .129, 91 .145, 139 .161, 89	.153, 293 .194, 228 .275, 452 .278, 404	.266, 1090 .276, 314 .392, 1055 .154, 69
8.9 Aperture Data for 5.8/ 0.57M	P4 P5 P6	.442, 26 .160, 100 .147, 41	.927, 107 .043, 87 .423, 1000	.619, 179 .345, 140 .367, 208	.697, 75 .516, 222 .681, 576
8.8/.68				.101, 85 .251, 346 .216, 223 .159, 151	
10.7/.79				.106, 186 .267, 967 .231, 320 .159, 170	

The propagation characteristics of wavefronts passed through turbulent flows have been described by Hogge. The time average, far-field intensity distributions are obtained for flows resulting in Gaussian phase statistics. In addition, the phase statistics are assumed to be homogeneous and isotropic in space. The phase covariance function, R_ϕ, is simply characterized by a variance, $\sigma^2{}_\phi$, and a length scale, ℓ_o, in the Gaussian form

$$R_\phi(r) = \sigma^2{}_\phi e^{(-r/\ell_o)^2} \tag{10}$$

The phase integral scale is

$$L_o = \frac{\int_o^\infty C\phi(r)\, dr}{\sigma^2{}_\phi} = \frac{\pi}{2}\,\ell_o \tag{11}$$

or note $L_o \cong \ell_o$

Expressions are developed for the average far-field irradiance distribution relative to the diffraction limited distribution for strongly phase aberrated wavefront. Specifically σ^2 aero was determined from

$$\sigma^2 = \beta^2 \int_0^L \langle\rho(r)\rangle^2 \int_{-L}^{L-r} \frac{\langle\rho(r)\rho(r+\Delta r)\rangle}{\langle\rho(r)\rangle^2}\, d\Delta r dr \tag{12}$$

where the kernel of the second integral is the correlation coefficient that is fitted with an exponential and when integrated yields the aerodynamic correlation length. β^2 is the Gladstone Dale constant. $\langle\rho(r)\rangle$ was determined from the differential form of the equation of state $P = \rho RT$. The data was recorded analog from steady-state through 100 hz. Corrections ($\sim$5% effect) to the data are required because the

density variation does not null due to coarse spatial sampling near the aircraft surface. The data thus calculated are the infinite aperture values of the spatial variances and deviation assuming homogeneity across the aperture.

The rationale for the finite aperture correlation follows. The size of the aperture physically describes the largest mode in the flow that can be observed. Any wavelength twice the size of the aperture diameter or larger is seen only as tilt, which is removed. Intuitively it can be seen that as the diameter shrinks the variance in the flow becomes less and thus the Strehl ratio approaches unity or the diffraction limit. At the other limit, as the diameter gets larger, the variance approaches that in the flow where the loss mechanics is that of wide angle scattering. Stated another way, the phase distortion is of high frequency compared to the aperture size. For beam apertures of the same order as the length scale of the phase distortion, the theory predicts an improved Strehl ratio. For such intermediate aperture sizes, the phase aberration results in wide angle scattering, narrow angle scattering, and tilt, where the wide angle scattering is caused by high frequency components in the phase spectrum, the narrow angle scattering is caused by length scales in the phase spectrum of the same order as the Strehl ratio is computed from the optical data using the exponential relation. This is shown in Figure 4. The theory developed by Dr. Hogge (Ref. 5) shows how the Strehl ratio observed in a finite aperture is related to the infinite aperture Strehl. It should be noted that it is not just size of the aperture that varies the Strehl

FIGURE 4

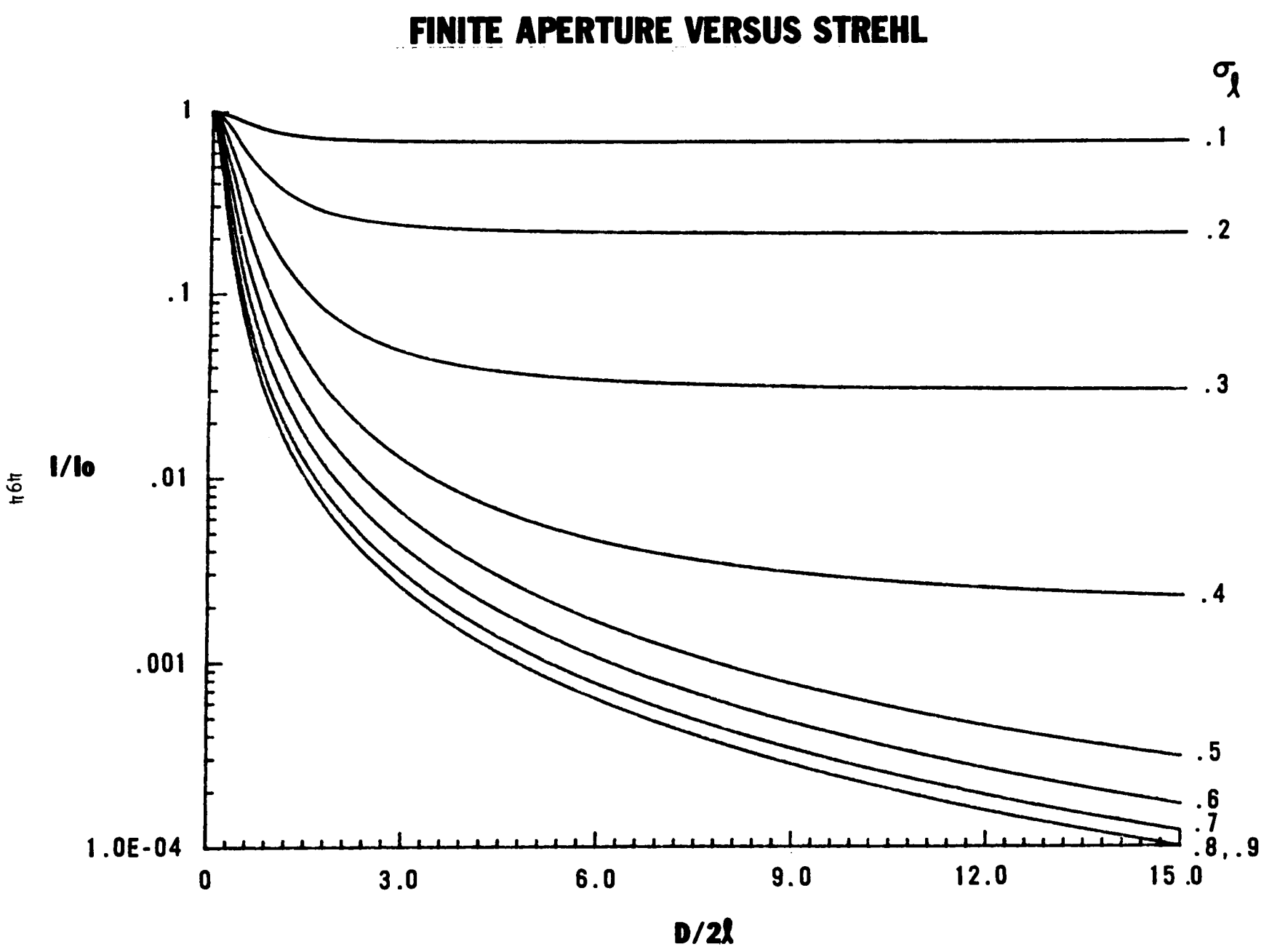
FINITE APERTURE VERSUS STREHL
σ_λ
.1
.2
.3
.4
.5
.6
.7
.8, .9
1
.1
.01
.001
1.0E-04
I/Io
0
3.0
6.0
9.0
12.0
15.0
D/2ℓ

but also the size of the correlation length.

Figure 5 compares the raw finite aperture data with the theory and the aerodynamic data. The plot shows Strehl or intensity ratio as a function of aperture radius times the correlation length of the flow. The three curves are the experimentally determined aerodynamic phase deviation at infinite aperture for the near, mid, and far fence condition (.252, .262, .904 σ respectively). The curves approach a Strehl of one as the aperture is decreased according to Dr. Hogge's theory. The data points show the optical data with piston and tilt removed. Therefore one expects them to be slightly greater than the respective point on the curve. It is of interest to note that for both the near and mid fence, the largest (15 cm aperture) optical data incorporates about 75% of all the flow contribution. (Compare the Strehl at $D/2 \cdot \ell = 2$ with the asymptotic value at 15.) It is for this reason we assert an increase of .15 m optics to 1 m optics will not necessarily degrade the Strehl much more. However, if the measurement point is on the order of 2 m aft of the fence, the degradation can be substantial. (see the far fence data)

Consider now the .16 wave tilt comment on the plot. The infinite aperture deviation for the mid fence calculated from the aerodynamic data is .262. When theoretically clipped the deviation is reduced to .238. The optical deviation is .210 with corresponding Strehl. Remembering that the variance is an infinite sum of Zernike polynomials, the optical measurement is the sum of P4 and up. Using the clipped aero data and the optical measurement and assuming no piston

FIGURE 5

STREHL VERSUS FINITE APERTURE

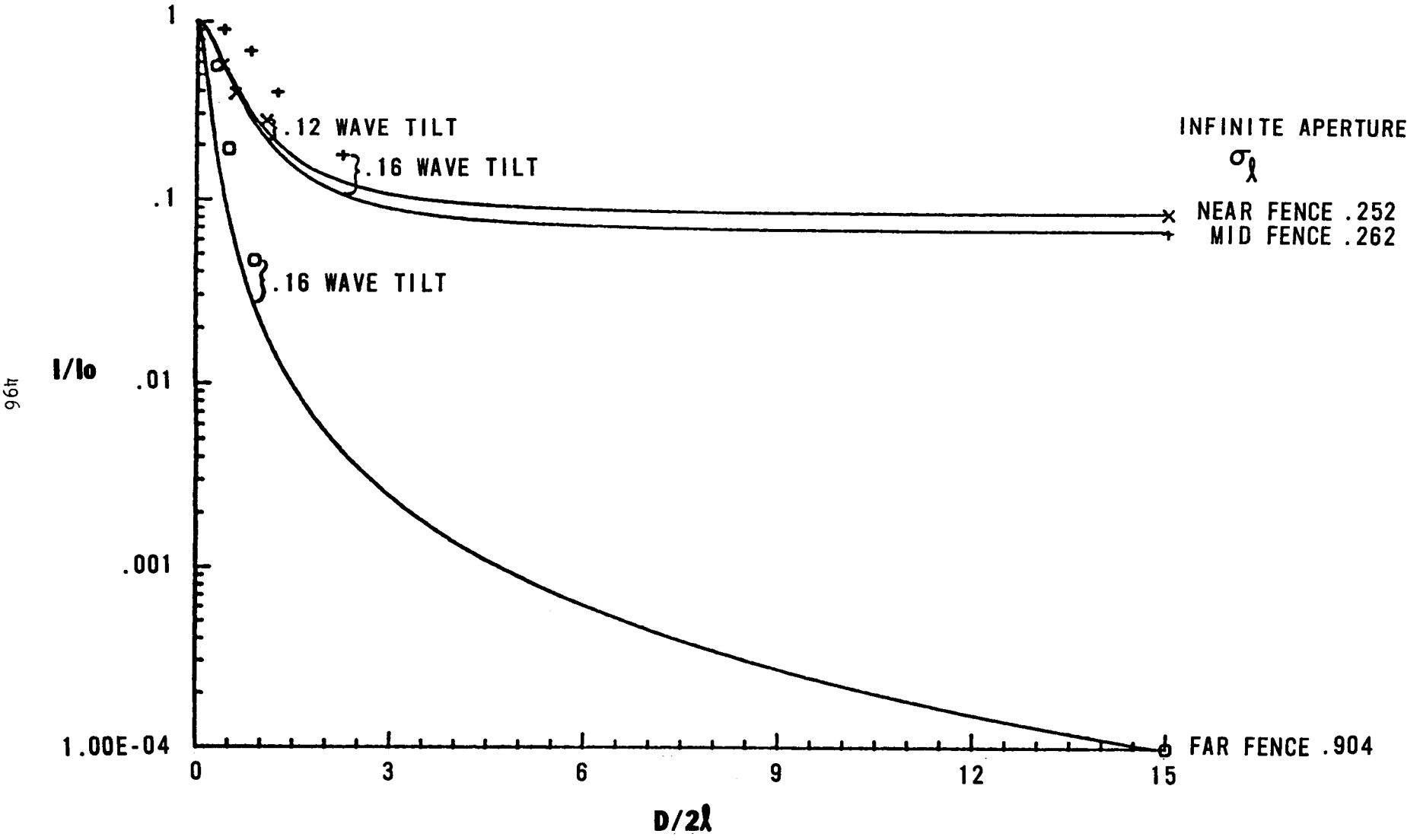

and equal X and Y tilt, a tilt coefficient can be calculated. This calculates to the .16 wave term listed. It is of interest that most data regardless of fence position or altitude yields tilt terms on the order of .2 waves which is the same order as the focus, astigmatism and tilt terms.

Extending the analysis a final step, one may consider the time sensitive aerodynamic temperature data. It is composed of a spectrum of frequency data which is transformed into density fluctuations and ultimately seen as turbules of various sizes. By clipping the frequency spectrum of all frequencies 0 to an f_c, all density fluctuations Vc/fc or greater are removed. V_c is the convection velocity of the flow (assuming $V_c = \lambda f$). This clipping technique removes the effect of the larger turbules on the optical variance and Strehl much like that of the finite aperture optical measurement with tilt removed. What is needed is correlation of the cutoff frequency with the Zernike polynomials tilt, focus, astigmatism or coma.

As a first attempt at correlation the following physical model is proposed. A turbule of size D where D is the optical aperture diameter is modelled as a convex lens of near perfect focus. Focus can be thought of as sinusoidal from 0 to π. Therefore a wavelength must be twice D or for this case 30 cm. To obtain the cutoff frequency of the aerodynamic data requires fixing a convection velocity which is sharply increasing across the shear layer. Time correlated data across the five probe rake requires use of an average convection velocity. That average was taken at .8 velocity halfway between the end probes, thus

f_c was determined. The density data was then clipped of all frequencies 0 to f_c. Then the density variation and correlation lengths were recalculated just as with the complete data set. The correlation length thus determined closely matched the optically calculated value at 2 cm derived above.

The variance also was shown to be consistent with the optical data. To understand this, consider first the form of the Zernike polynomials.

$\rho \cos \theta$; $\rho \sin \theta$	tilt	ρ terms
$2\rho^2-1$	focus	ρ^2 term
$\rho^2 \cos 2\theta$; $\rho^2 \sin \theta$	astigmatism	ρ^2 term
$(3\rho^2-2)\rho \cos \theta$; $(3\rho^2-2) \rho \sin \theta$	coma	ρ^3 terms

Tilt translates the image, focus converges (diverges) the image, astigmatism is one-dimensional focus causing nonlinear convergence as the axis is rotated, coma adds third order distortion. It is obvious that the first attempt correlate turbule size has some error. In fact for a turbule of size D has all ρ^2 terms, not just pure focus. Turbules of size 2D centered in the aperture can likewise yield a focus contribution. Only when these turbules are off center do they approximate the tilt or ρ terms. Therefore clipping all λ that are 2D and greater removes some focus and astigmatism components resulting in a variance (deviation) greater than the optical σ_{0-8} and less than σ_{0-2}. By using the aerodynamic data for the middle probe only matching the convection velocity with clipped density profile results

in a $\sigma_{CLIPPEDAERO} = .144$. By using the aerodynamic data for all five probes with the average velocity it can be shown the effect of the error of using that velocity instead of the actual velocity at the probe point is to clip some turbule data at 75% of D which seems to include ρ^3 Zernike component. This can be visualized comparing figure 6 a and b. The data tends to confirm this theory.

$\sigma_{\infty aero} = .25\ \lambda$

$\sigma_{opt0\text{-}2} = .20\ \lambda$

$\sigma_{aero}{}^{\lambda>}{}_{2D} = .144\ \lambda$

$\sigma_{aero}{}^{\lambda>}{}_{1.5D} = .13\ \lambda$

$\sigma_{opt0\text{-}8} = .12\ \lambda$

Thus we conclude for turbules > 4D aperture size, the effect of the aperture is to basically remove tilt; for turbules 3/4 to 2D, the effect is tilt, focus and astigmatism removal; for turbules 1/2 to 3/4D, the effect is tilt through coma removal. This matches the comparison of aerodynamic and optical deviations given. Therefore the spatial correlation between aerodynamic and optical measurement is confirmed.

As a final note in this experiment, 1/2 the data was taken with horizontally induced fringes and 1/2 with vertically induced fringes. It is noted that the deviations obtained from the flow wise interferograms matched those of the normal fringe interferograms. This says for aerodynamic flows, that 20 or so fringes across an interferogram is accurate enough not to perturb the statistical results. Further a study of up to 100 interferograms per condition showed that an ensemble

FIGURE 6a Zernike Polynomials

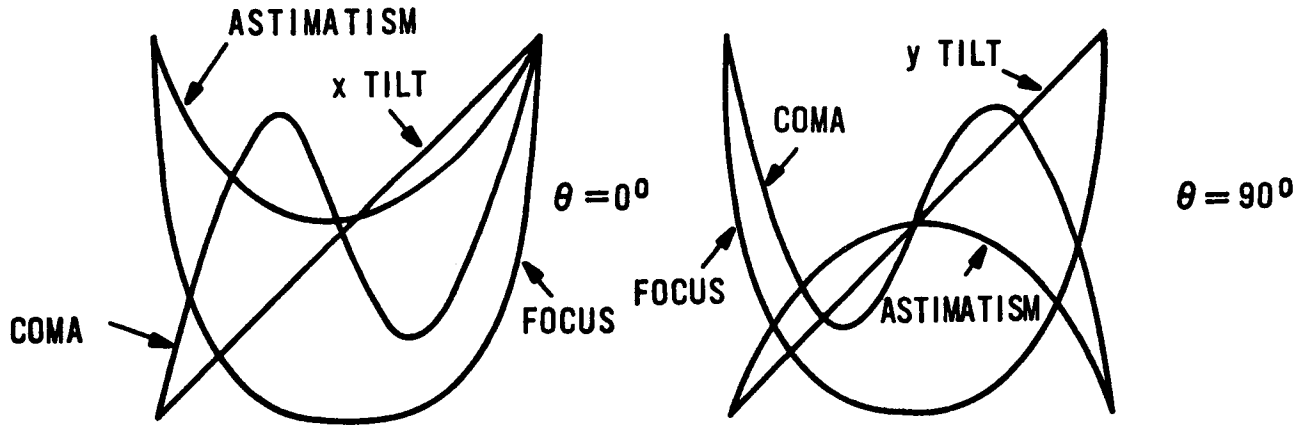

FIGURE 6b Turbule Size Versus Aperture

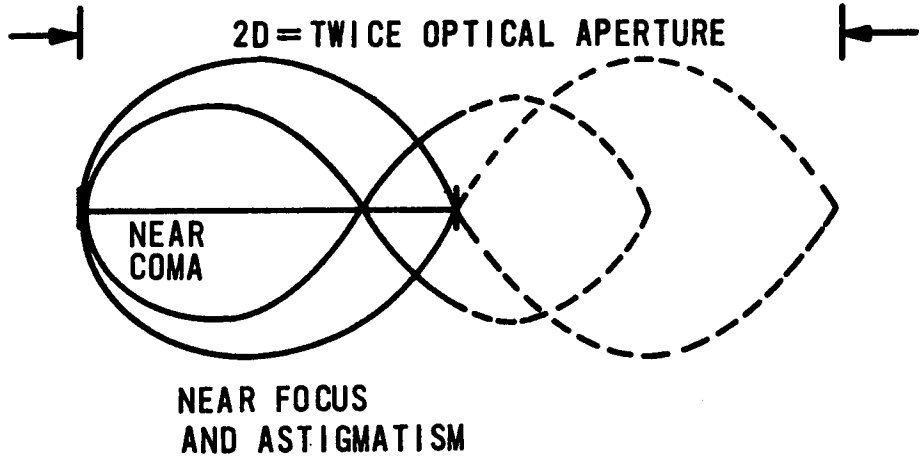

of 15 random holograms yielded statistically equal results. Finally a procedure, for which Rocketdyne Corporation can be truly proud, automated interferogram reduction so that they averaged 40 interferograms reduced per day and peaked at 70 per day. This capability will allow follow-on experiments near next day turnaround of much data.

ACKNOWLEDGEMENTS

This work was done under various contracts between the Air Force Weapons Laboratory and Rocketdyne Corporation, General Dynamics, Rose Engineering, and Spectron Development Laboratories. The authors acknowledge the outstanding team work of the contractors, with 4950th Aerospace Test Wing and AFWL computing center collecting and processing the data, and Maj Gary Lynch, Capt John Waskiewicz, Lt Jeff Laughlin, Lt Skip Gresko, Mr. Eric Helfer, Brian Kennedy and Ms Debra Temer of the Air Force Weapons Laboratory in reducing the data.

REFERENCES

1. Gilbert, K.G., "KC-135 Aero-Optical Turbulent Boundary Layer/Shear Layer Experiments," Proceedings from Joint USAF/NASA Aero-Optics Symposium on Electromagnetic Wave Propagation from Aircraft, NASA CP 2121 National Aeronautics and Space Administration, Moffett Field, CA, April 1980.

2. Craig, J.E., Trolinger, J.D. and Rose, W.C., "Propagation Diagnostic Techniques for Turbulent Transonic Flow," Proceedings from AIAA 22nd Aerospace Science Meeting AIAA-84-0104, American Institute of Aeronautical Astronautics, January 1984.

3. Rose, W.G., Optical Effects of Near-Field Turbulence About a Small-Scale Turret Model, AFWL TR-79-129, Air Force Weapons Laboratory, Kirtland AFB, NM, August 1979.

4. Rose, W.C., Measurements of Aerodynamic Parameters Affecting Optical Performance, AFWL TR-78-191, Air Force Weapons Laboratory, Kirtland AFB, April 1979.

5. Hogge, Charles B., Strongly Phase-Aberrated Nondiffraction Limited Laser Beam, AFWL TR-75-153, Air Force Weapons Laboratory, Kirtland AFB, January 1976.